



Towards 5G new radio sidelink communications: A versatile link-level simulator and performance evaluation

Peng Liu^{a,b,*}, Chen Shen^{a,c,1}, Chunmei Liu^a, Fernando J. Cintrón^a, Lyutianyang Zhang^d, Liu Cao^d, Richard Rouil^a, Sumit Roy^d

^a Wireless Networks Division, National Institute of Standards and Technology, 100 Bureau Dr, Gaithersburg, MD, 20899, USA

^b Prometheus Computing, LLC, 4977 Battery Lane #214, Bethesda, MD, 20814, USA

^c Department of Physics, Georgetown University, 37th and O Street NW, Washington, DC, 20057, USA

^d University of Washington, Seattle, WA, 98195, USA

ARTICLE INFO

MSC:

0000

1111

Keywords:

5G NR

Sidelink

Link-level simulator

Communication range

Feedback-based HARQ

ABSTRACT

Sidelink in cellular networks enables direct exchange of data packets between devices without the need for network infrastructure, resulting in various benefits, including communication in out-of-coverage areas and possible decrease in latency by a considerable extent. Thus, sidelink is a favorable choice for applications like public safety communications and Vehicle-to-Everything (V2X) communications. As 4G Long Term Evolution (LTE) advanced to 5G New Radio (NR) under the Third Generation Partnership Project (3GPP), several new features were introduced to sidelink, such as two-stage Sidelink Control Informations (SCIs), data and control multiplexing, and feedback-based Hybrid Automatic Repeat Request (HARQ) with a configurable maximum number of transmissions. To conduct extensive NR sidelink link-level evaluations, a comprehensive simulation platform is essential. In this paper, we introduce the first publicly accessible 5G NR Link-Level Simulator (LLS) that supports major 5G NR sidelink features and complies with the 3GPP standards. This MATLAB-based simulator allows for flexible control over various Physical Layer (PHY) configurations, facilitating customized simulations on algorithm development and performance evaluations. We discuss the simulator's structure and the sidelink features implemented in detail and evaluate the 5G NR sidelink performance using the developed simulator. Our simulation results indicate that the Block Error Rate (BLER) curves are insensitive to error-prone 2nd-stage Sidelink Control Information (SCI2) and number of Resource Blocks (RBs) allocated; however, the sidelink communication range is sensitive to the deployment environment. We also highlight the need for a careful choice of numerology, device power class and HARQ configuration to balance performance metrics for a variety of services based on 5G NR sidelink deployment scenarios.

1. Introduction

The introduction of sidelink technology in cellular networks dates back to March 2015 when the Third Generation Partnership Project (3GPP) included it in Long Term Evolution (LTE) Device-to-Device (D2D) communications. Unlike traditional cellular networks, sidelink allows devices to directly exchange data without the need to go through base stations and network infrastructure. This feature provides various advantages, such as enabling communication in out-of-coverage areas and potentially reducing latency by eliminating hops to, from, and within the network infrastructure. These benefits make sidelink communications an attractive option for multiple services, including Proximity Services (ProSe) in public safety communications and Vehicle-to-Everything (V2X) communications, leading to extensive research in this area [1,2].

With the advancement of technology from 4G LTE to 5G New Radio (NR), starting from 3GPP Release 16, new features were introduced to sidelink to improve its performance and cater to various service needs [3,4]. These features include, but are not limited to, numerology (inherited from the Uu interface), sensing mechanism, two-stage Sidelink Control Informations (SCIs), feedback channel, and flexible maximum number of Hybrid Automatic Repeat Request (HARQ) transmissions. With the introduction of these new features, simulations could play a significant role in analyzing and evaluating 5G NR sidelink performance.

For wireless communication studies, simulators have been developed and widely used at different levels. These levels include link-level simulation, which evaluates Physical Layer (PHY) performance by Block Error Rate (BLER), Bit Error Rate (BER), or Frame Error

* Corresponding author at: Prometheus Computing, LLC, 4977 Battery Lane #214, Bethesda, MD, 20814, USA.

E-mail address: peng.liu@nist.gov (P. Liu).

¹ Now at Google.

Rate (FER) under controlled PHY parameters and environment [5–7]; system-level simulation, which assesses system performance under various system environments, such as scheduling strategies, frequency bands, and deployment configurations [8–10]; and network-level simulation, which considers various network components, such as core network and radio access networks, and focuses on network performance [10–13]. Among these simulations, link-level simulations are widely used to simulate point-to-point communication links and PHY performance, and are often used to provide inputs to system-level simulations such as BLER curves.

Specific to LTE and NR, there are two primary suites of Link-Level Simulators (LLSs) available that offer a rich set of PHY modules and are adaptable for reuse. One suite is developed by MathWorks² For LTE, MathWorks developed an LTE toolbox that supports Downlink (DL), Uplink (UL) and Sidelink (SL) [5]. Accordingly, LLSs can be built using the tools provided. For sidelink in particular, MathWorks provides tools for Release 12 ProSe transmission mode 1 and mode 2, as well as Release 14 V2X transmission mode 3 and mode 4. Similarly, for NR, MathWorks developed a 5G toolbox that is compliant with 3GPP Release 15. However, while it supports both downlink and uplink, sidelink is not available at the time of writing. Another LLS suite is provided by the Vienna Cellular Communications Simulators,¹ which offers a range of link-level and system-level simulators for both 4G LTE and 5G NR [7]. Its 5G LLS supports downlink and uplink and provides high flexibility in controlling a broad range of parameters. However, similar to MathWorks, sidelink support is currently not available. While there are other simulators mentioned in the literature [9,14], to the best of our knowledge, there is no publicly accessible NR SL LLS yet.

In this paper, we introduce the 5G NR SL LLS that we have developed for the study of NR sidelink technology [15], aimed at meeting the simulation needs for this rapidly developing area and filling the existing gap. The simulator is MATLAB based. Instead of developing NR SL LLS from scratch, we utilized the rich set of PHY modules from Vienna DL and UL LLS and MathWorks 5G toolbox, and focused on the development of NR sidelink specific features. We reused general LLS software structure and some basic functionalities from Vienna LLS, and channel coding from MathWorks 5G toolbox. The NR sidelink features developed include, but are not limited to, sidelink Bandwidth Part (BWP) and resource pool, sidelink slot format including feedback channel and two-stage SCIs, data and control multiplexing and scrambling, sidelink layer mapping and precoding, and blind and feedback-based HARQ. In this paper, we also present a variety of simulation results that prove the successful development of our simulator.

The simulator follows closely Release 16 of 3GPP 5G NR sidelink specifications, and has a highly flexible structure that is easy to adapt to various NR sidelink link-level simulations of interest. The simulator also keeps the branches of DL and UL LLS, so that it supports all DL, UL, and SL LLS. The current release focuses on one point-to-point NR sidelink and data transmissions. To the best of our knowledge, this simulator is the first 5G NR SL LLS that is publicly accessible.

In addition, in this paper we also use the developed 5G NR SL LLS to evaluate 5G NR sidelink performance. As one major function of link-level simulations and to facilitate the link-to-system mappings, we start with the impact of error-prone 2nd-stage Sidelink Control Information (SCI2) and number of allocated Resource Blocks (RBs) on sidelink BLER curves. After that, we analyze the performance of sidelink, including communication range, throughput, and latency. The factors evaluated include deployment environment, numerology, device power class,

² Certain equipment, instruments, software, or materials, commercial or non-commercial, are identified in this paper in order to specify the experimental procedure adequately. Such identification is not intended to imply recommendation or endorsement of any product or service by National Institute of Standards and Technology (NIST), nor is it intended to imply that the materials or equipment identified are necessarily the best available for the purpose.

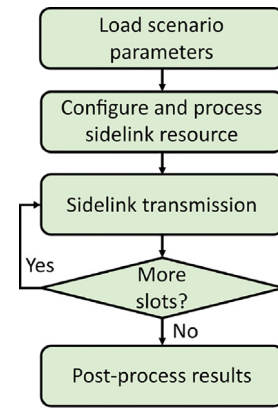


Fig. 1. Basic Simulator Structure.

and blind/feedback-based HARQ with multiple maximum number of transmissions.

The rest of the paper is organized as follows. In Section 2 we introduce the simulator structure and supported features. In Section 3 we dive into NR sidelink features developed in detail. In Section 4 we present simulation results using the simulator. And finally we present our concluding remarks in Section 5.

This paper extends the previous introduction to the NR SL LLS and the corresponding simulation results [16]. With the progression of the simulator, new features were developed and more contributions are made:

- We expand the function of pathloss-to-distance conversion to the evaluation of communication range and other performance metrics, which include but are not limited to target Signal-to-Noise Ratio (SNR), throughput, and latency (Section 3.8).
- We provide a generalized method to manage the constants that comply with 3GPP standards as well as add new constants (Section 3.9).
- We offer a convenient tool to adaptively identify the range of an input simulation parameter (Section 3.10).
- We evaluate the impact of the number of RBs allocated and find that its impact on BLER curve shift is insignificant (Section 4.2).
- We quantify communication ranges under various deployment environment with different Power Delay Profiles (PDPs) (Section 4.3).
- We extend the scope of sidelink performance research to consider changes, in both, numerology and User Equipment (UE) power class. The improvements in communication range at higher power class are also quantified (Section 4.4).

2. Simulator structure and supported features

The 5G NR SL LLS inherits the structure from Vienna 5G NR LLS, including its main functionalities [7]. A basic simulator structure is presented in Fig. 1. The simulator starts by loading a scenario profile containing the setup of two UEs and a link object that represents the connection between the two UEs. Transmission parameters are also specified, including but not limited to, antenna configurations, precoding matrix, channel coding scheme, waveform, channel model, and equalizer. Next, the *SL_BWP* object is created according to the scenario parameters, and the time slots where the Sidelink Synchronization Signal Blocks (S-SSBs) are transmitted are also derived. Afterward, a slot-by-slot simulation with a sweep parameter is performed for a specified number of slots. Finally, the results of interest are post-processed.

Typically, most LLSs fix the SNR as input parameter. Instead, Vienna 5G LLS fixes the transmit and noise power, and sets the path loss as

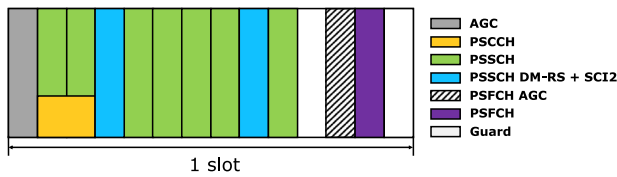


Fig. 2. Generic 5G NR sidelink Slot Format.

an input parameter of the simulator [7]. We inherited this structure in the SL LLS. In addition, Vienna 5G simulator generates throughput, BER, and FER as PHY performance metrics. While we kept them for the downlink and uplink branches, for sidelink, we generate throughput, packet loss rate, and latency as performance metrics, and have plans to include BER and FER in future releases. Note that since the focus of link-level simulations is on physical layer, latency here refers to the difference from the time a data packet is transmitted at the transmitter to the time it is received successfully at the receiver. It is a simplified version and does not include other delays such as processing delay. Monte Carlo simulations are then carried out and results are averaged over a certain number of channel, noise, and data realizations.

For sidelink in particular, Fig. 2 illustrates the sidelink slot format with 2-symbol Physical Sidelink Control Channel (PSCCH), 2-symbol Demodulation Reference Signal (DM-RS) for Physical Sidelink Shared Channel (PSSCH), and Physical Sidelink Feedback Channel (PSFCH). The slot formats corresponding to other settings are similar, and will be discussed in detail in Section 3. As the focus of the sidelink simulator in this release is on data channel, PSCCH and PSFCH are assumed to be error-free. That is, there is no loss on 1st-stage Sidelink Control Information (SCI1), Acknowledgements (ACKs), and Negative Acknowledgements (NACKs). Accordingly, dummy symbols with unit power are used to fill the Resource Elements (REs) for PSCCH and DM-RS. Meanwhile, Automatic Gain Control (AGC) and guard symbols are implemented per the 3GPP TS 38.211 [17].

Specific to PSSCH, which is the channel that carries data, Fig. 3 illustrates the processing chain at the transmitter and receiver sides. While the basic steps are similar to typical processing chains, there are multiple blocks that are specific to 5G NR sidelink.

First, SCI messages in 5G NR sidelink are transmitted in two stages, SCI1 and SCI2. While SCI1 is included in the PSCCH, SCI2 is multiplexed together with data and transmitted over PSSCH [18]. Moreover, different schemes are applied to SCI2 and data. SCI2 goes through Polar coding and Quadrature Phase Shift Keying (QPSK) modulation, while data goes through Low Density Parity Check (LDPC) coding and a selected modulation scheme from a set of Modulation and Coding Schemes (MCSs) [17]. Hence, sidelink requires its own processing, including separate coding, specific scrambling, separate constellation modulation, and specific layer mapping. The sidelink simulator implements these processes by closely following 3GPP, as shown in Fig. 3, at both the transmitter side and the receiver side. It is worth noting that, since the focus of this release is on data, dummy bits instead of the actual fields of SCI2 are used as SCI2 content, and these dummy bits then go through the processing chain. The simulator provides the flexibility to simulate and evaluate both error-free SCI2 and error-prone SCI2.

Second, 5G NR sidelink supports up to two layer spatial multiplexing, which allows reuse of the resource grid shown in Fig. 2. The simulator supports this specific resource grid (sidelink slot format in Section 3.2) and the corresponding layer mapping.

Third, 5G NR sidelink supports both blind-based and feedback-based HARQ mechanisms, with a configurable and up to 32 maximum number of transmissions. While it is assumed that the feedback channel is error-free and the content of PSFCH is not implemented, the simulator supports both PSFCH mechanisms following 3GPP [19], including feedback period and minimum gap.

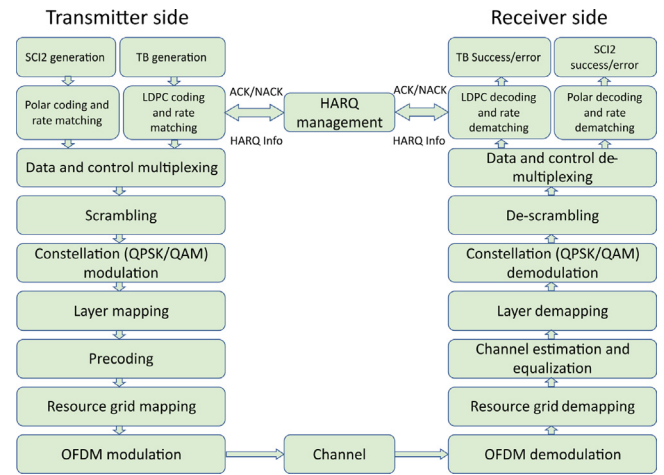


Fig. 3. Transmitter and Receiver Processing Chain.

Table 1

Supported features by the simulator.

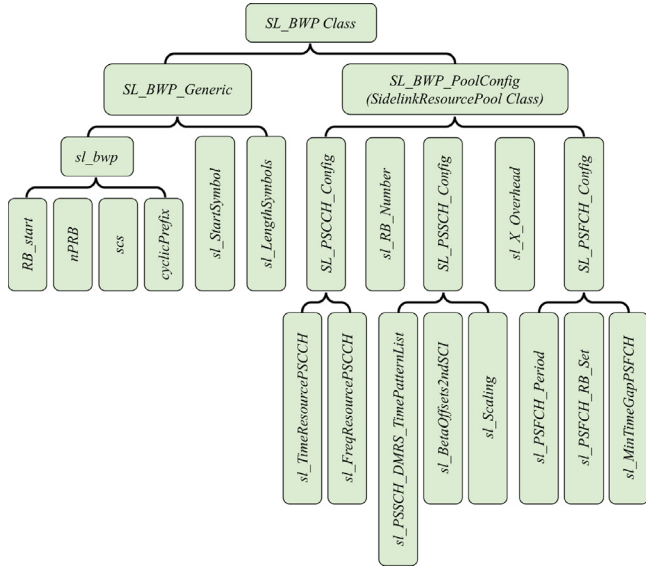
Inherited features	Developed features
General functionality	Sidelink BWP and resource pool
Channel coding	Sidelink slot format
Channel models	Data and control multiplexing
Channel estimation	Data and SCI2 scrambling
Modulation	Sidelink layer mapping and precoding
Equalization and detection	Error-free and error-prone SCI2
	Blind- and feedback-based HARQ
	Communication range and performance evaluation
	Constant management
	Adaptive sweeping value selection

The simulator also supports other 5G NR sidelink features, such as sidelink BWP, resource pool, and identity precoding matrix [20], together with communication range and other performance evaluation. Table 1 summarizes the features reused from Vienna 5G simulator and MathWorks, and the features developed specifically for sidelink. In Section 3 we detail these features with a focus on the developed ones.

3. Simulator features

The inherited features from Vienna NR UL and DL LLS and MathWorks 5G toolbox provide general functionalities to the NR sidelink implementation. To develop the NR SL LLS, however, the sidelink-specific configurations for these functionalities, as well as the sidelink-only features, still need to be comprehensively implemented. Such features are developed following 3GPP specifications across different NR sidelink protocol stacks, including sidelink bandwidth part and resource pool in Radio Resource Control (RRC), blind- and feedback-based HARQ transmissions in Medium Access Control (MAC) and PHY, data and control multiplexing and scrambling, layer mapping and precoding, and sidelink slot structure in PHY. Furthermore, to facilitate the simulation and data acquisition, the selection between error-free and error-prone SCI2 is implemented. Other supported features include conversion from pathloss to communication range and other performance metrics, management of 3GPP standards constant values, and adaptive sweeping that automatically selects the SNR range for simulations.

To ensure adequate functionality, flexibility, and correctness of the sidelink simulator, the development of sidelink features complies with 3GPP Release 16 specification, while the structures of some parameters are modified to offload the configuration complexity without affecting their correctness. In the following subsections, we introduce each of the sidelink features developed.

Fig. 4. Structure of the *SL_BWP* class.

3.1. Sidelink bandwidth part and resource pool

3.1.1. Sidelink bandwidth part

The BWP for sidelink differs from those for uplink or downlink in that a UE can be configured with only one BWP for sidelink [19], whereas up to four uplink or downlink BWPs can be configured [17]. The sidelink BWP for a UE-specific NR sidelink communication is specified by the Information Element (IE) *SL-BWP-Config* in the RRC protocol [20]. It contains two major IEs:

1. *sl-BWP-Generic-r16*, which configures the generic sidelink BWP time and frequency resources, and
2. *sl-BWP-PoolConfig*, which configures the sidelink resource pool.

The structure of the sidelink BWP class, as well as its relation to the sidelink Resource Pool class, is illustrated in Fig. 4.

The Subcarrier Spacing (SCS) (*scs*) is related to the numerology (μ):

$$scs = 15 \times 2^\mu \text{ kHz}, \quad (1)$$

and *scs* can only be 15 kHz, 30 kHz, or 60 kHz in Frequency Range 1 (FR1), and 60 kHz or 120 kHz in Frequency Range 2 (FR2) [20].

The cyclic prefix (*cyclicPrefix*), which can be normal or extended, defines the number of Orthogonal Frequency-Division Multiplexing (OFDM) symbols in a slot (*nSymbol*). extended applies only when $\mu = 2$ [17]. *nSymbol* is 14 and 12 when *cyclicPrefix* is normal and extended, respectively. The index of the start symbol (*sl_StartSymbol*) and the length of the sidelink symbols in a slot (*sl_LengthSymbols*) can be configured by meeting the following condition:

$$sl_StartSymbol + sl_LengthSymbols \leq nSymbol. \quad (2)$$

To configure the start index of the RBs (*RB_start*) and the number of RBs for the sidelink BWP (*nPRB*), we need to first acquire the maximum transmission bandwidth configuration in unit of RB (*maxRB*). *maxRB* is jointly determined by *scs* and the selected bandwidth, which is specified in Table 5.3.2-1 of [21] for FR1 or Table 5.3.2-1 of [22] for FR2. In addition, to ensure the configuration does not exceed *maxRB*, the following condition needs to be met:

$$RB_start + nPRB \leq maxRB. \quad (3)$$

3.1.2. Sidelink resource pool

The IE *sl-BWP-PoolConfig* specifies sidelink resource pool configuration. The sidelink resource pool updates every 10 240 ms, and provides configurations for PSCCH, PSSCH, and PSFCH. In the SL LLS, these configurations are stored using the *SidelinkResourcePool* class, as illustrated in Fig. 4.

In each sidelink slot, two or three OFDM symbols can contain PSCCH, and the PSCCH can occupy 10, 12, 15, 20, or 25 Physical Resource Blocks (PRBs) [20]. The time and frequency resources allocated to PSCCH are defined by *sl_TimeResourcePSCCH* and *sl_FreqResourcePSCCH*, respectively.

In PSSCH, the number of OFDM symbols that contain DM-RS can be 2, 3, or 4, which is indicated by *sl_PSSCH_DMRS_TimePatternList*. *sl_TimeResourcePSCCH*, *sl_PSSCH_DMRS_TimePatternList*, and the number of OFDM symbols for PSSCH jointly determine the OFDM symbols that contain PSSCH DM-RS, using Table 8.4.1.1.2-1 in [17]. *sl_BetaOffsets2ndSCI* corresponds to the length of the coded SCI2 modulation symbols [20], and *sl_Scaling* provides the upper bound ratio of the number of coded SCI2 modulation symbols over the total number of REs for PSSCH transmission. Both of them are used in the rate matching of the coded SCI2 bits [18].

In cases where feedback-based HARQ is enabled, *SL_PSFCH_Config* is configured. The PSFCH is transmitted on the dedicated sidelink slots with a periodicity of 1, 2, or 4 slots [20], which is configured by *sl_PSFCH_Period*. On reception of a PSSCH, the receiver waits for at least 2 or 3 slots of the resource pool before checking for an available PSFCH. This gap of slots is configured by *sl_MinTimeGapPSFCH*. The modulation symbols of the feedback information in the corresponding slot(s) and subchannel(s) are mapped to the RB set of *sl_PSFCH_RB_Set* [19]. As shown in Fig. 6, when the PSFCH is to be transmitted, the OFDM symbol for PSFCH, as well as those for the PSFCH AGC that precedes it and the guard symbol that follows it, occupy the last three OFDM symbols of the sidelink slot.

It is worth mentioning that most of the configurations follow the 3GPP standards, while some parameters are simplified. For example, instead of having multiple configurations, each of *sl_PSSCH_DMRS_TimePatternList* and *sl_BetaOffsets2ndSCI* have only a single value. Also, in *sl_BetaOffsets2ndSCI*, we record the actual Beta offset value, instead of the lookup index for Table 9.3-2 of [19]. Another modification is that instead of subchannels, the frequency resources in the sidelink resource pool is configured based on the number of RBs *sl_RB_Number*. Such changes were made to simplify the configuration structure without loss of accuracy.

3.2. Sidelink slot format

As introduced above, a sidelink slot can contain 12 or 14 OFDM symbols in the time domain, depending on the cyclic prefix and SCS configurations. In frequency domain, (10 to 275) RBs can be configured, whereas the actual RB number is constrained by *nPRB* in sidelink BWP and eventually *sl_RB_Number* in sidelink resource pool. Each RB contains 12 subcarriers. The basic resource unit is an RE, which occupies one OFDM symbol in the time domain and one subcarrier in the frequency domain. An RE contains one modulation symbol for a physical channel or a reference signal.

A sidelink slot can contain (1) the physical channels of PSSCH, PSCCH, and PSFCH, and (2) the reference signals of DM-RS, Channel-State Information Reference Signal (CSI-RS), and Phase-Tracking Reference Signal (PT-RS). The PSSCH contains symbols of SCI2, data, and DM-RS, and the PSCCH contains symbols of SCI1 and DM-RS. In this simulator, we implemented the mapping of PSSCH, PSCCH, and PSFCH symbols for their corresponding elements, whereas the implementation of CSI-RS and PT-RS was left for future development.

In a sidelink slot, the first OFDM symbol starts at the symbol with index *sl_StartSymbol*, as specified in the sidelink BWP. This symbol is used for AGC [3], and it is a duplication of the following OFDM

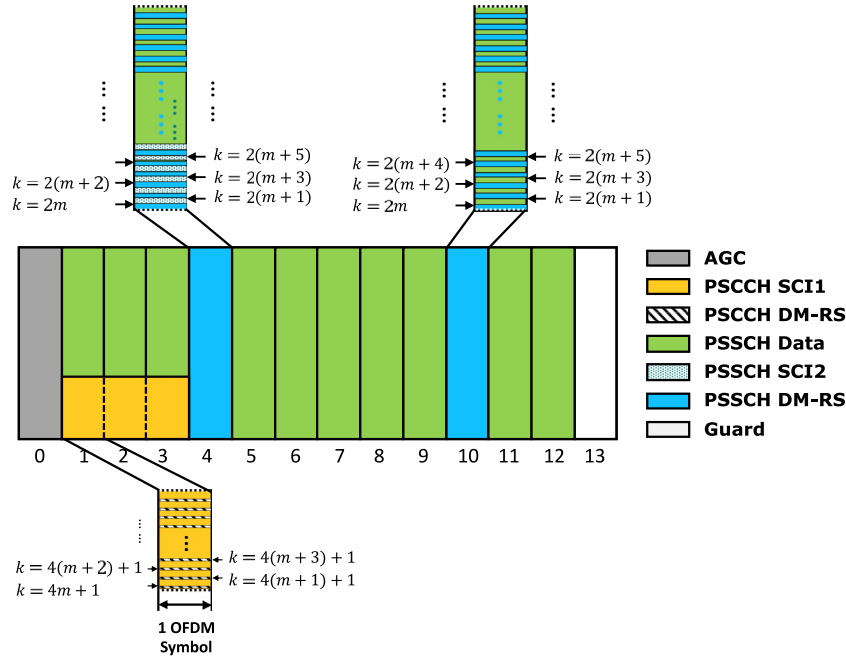


Fig. 5. A sidelink slot without PSFCH. $sl_StartSymbol = 0$, $sl_LengthSymbols = 14$, $sl_TimeResourcePSCCH = 3$, and $sl_PSSCH_DMRS_TimePatternList = 2$.

symbol [17]. The PSCCH is mapped to the OFDM symbols starting at index $sl_StartSymbol + 1$, and its resources are specified by $sl_TimeResourcePSCCH$ and $sl_FreqResourcePSCCH$. In the REs assigned to PSCCH, the symbols for the PSCCH DM-RS are mapped to the REs with index (k, l_0) :

$$k = 4m + 1, m = 0, 1, 2, \dots, \quad (4)$$

$$l_0 = sl_StartSymbol + 1, \dots, \quad (5)$$

$$sl_StartSymbol + sl_TimeResourcePSCCH,$$

where k is the RE index in the frequency domain, and l_0 is the index of the OFDM symbol in a slot. The modulation symbols for SCI1 are mapped to the remaining REs for PSCCH.

The modulation symbols for PSSCH DM-RS, SCI2, and data are mapped to their corresponding REs in the following order:

- Mapping of PSSCH DM-RS symbols,
- Mapping of SCI2 symbols, and
- Mapping of data symbols.

The indexes of the OFDM symbols that contain PSSCH DM-RS are determined using Table 8.4.1.1.2-1 of [17], where

$$\bar{l} = l_0 - sl_StartSymbol, \quad (6)$$

$$l_d = \begin{cases} sl_LengthSymbols - 1 & \text{if no PSFCH in slot,} \\ sl_LengthSymbols - 4 & \text{if PSFCH in slot,} \end{cases} \quad (7)$$

where the number of PSSCH DM-RS is specified by $sl_PSSCH_DMRS_TimePatternList$. Figs. 5 and 6 illustrate the PSSCH DM-RS symbol assignments in two different sidelink configuration scenarios. In each of these OFDM symbols, the PSSCH DM-RS modulation symbols are assigned to the REs with $k = 2m$, where $m = 0, 1, \dots$ and k does not exceed the allocated number of REs.

The SCI2 modulation symbols are mapped to the vacant REs starting at the lowest index in first OFDM symbol that contains PSSCH DM-RS, where $k = 2m + 1$. If additional REs are necessary, the vacant REs in the following OFDM symbol(s) will be utilized. The locations of the SCI2 symbols are detailed in Figs. 5 and 6 as well.

In a sidelink slot without PSFCH, the OFDM symbol with index $sl_StartSymbol + sl_LengthSymbols - 1$ functions as a guard symbol. All

the vacant REs from index $sl_StartSymbol + 1$ to $sl_StartSymbol + sl_LengthSymbols - 2$ are utilized for mapping of PSSCH data.

In a sidelink slot with PSFCH, the OFDM symbols with indexes $sl_StartSymbol + sl_LengthSymbols - 4$ and $sl_StartSymbol + sl_LengthSymbols - 1$ are guard symbols. All the vacant REs from index $sl_StartSymbol + 1$ to $sl_StartSymbol + sl_LengthSymbols - 5$ are utilized for mapping of PSSCH data. The OFDM symbol at index $sl_StartSymbol + sl_LengthSymbols - 2$ contains the PSFCH, and the assigned REs are specified by $sl_PSFCH_RB_Set$. The OFDM symbol that precedes it is its duplication and functions as the AGC for PSFCH.

The mapping of all the modulation symbols for each of the physical channels and reference signals starts from the lowest indexes of k and l_0 , and the symbols occupy the corresponding REs in increasing order of first k and then l_0 .

The functions of the $SL_SlotStructure$ class are illustrated in Fig. 7. The constructor function $SL_SlotStructure$ retrieves the parameters that are related to the slot structure configuration from SL_BWP and its resource pool, as well as the number of Multiple-Input and Multiple-Output (MIMO) layers ($nLayer$) and the enabling of PSFCH in this slot ($PSFCH_overhead_indication$). Based on the configuration, the elements for different physical channels and reference signals are tagged in a matrix by using different tag numbers. This function is realized by calling the $update_SlotStructMatrix$ function. The tags can be color coded and displayed using the $plot_SlotStructMatrix$ function. At the transmitter, the mapping of physical channels and reference signals follows the modulation of digital signals. Using the $map_PHY_Channels$ function, the modulation symbols for PSCCH SCI1, PSCCH DM-RS, PSSCH SCI2, PSSCH data, PSSCH DM-RS, and PSFCH can be mapped to the corresponding elements of the slot structure matrix. The $map_PHY_Channels$ function calls the individual functions for each physical channel or reference signals to complete such mapping, followed by duplicating the corresponding elements of PSCCH and PSSCH to the elements for AGC. At the receiver, after the OFDM demodulation, the modulation symbols are demapped by the $demap_PHY_Channels$ function. Each individual function that $map_PHY_Channels$ or $demap_PHY_Channels$ calls can also be utilized individually when symbols for a specific physical channel or reference signal need to be modified or extracted.

In the LLS, the slot structures for the transmitter and receiver are initialized whenever the link between nodes are updated. The mapping of the physical channels and reference signals to the transmitter slot

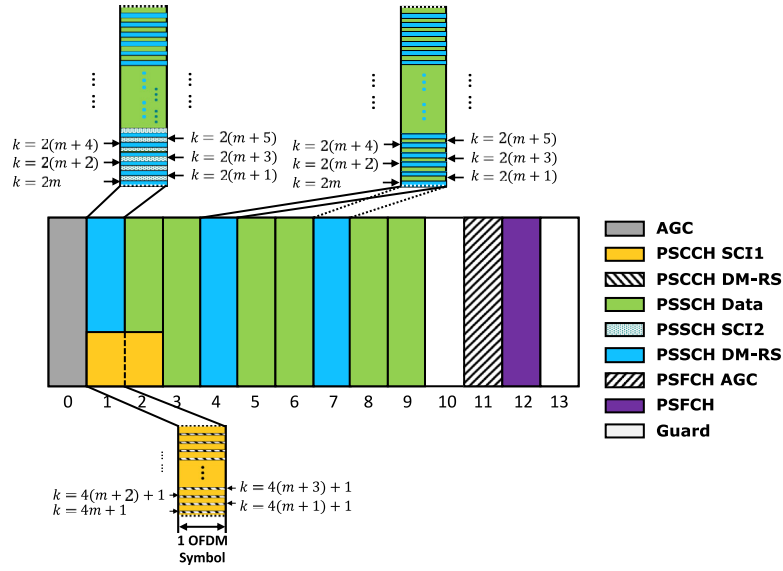


Fig. 6. A sidelink slot with PSFCH. $sl_StartSymbol = 0$, $sl_LengthSymbols = 14$, $sl_TimeResourcePSSCH = 2$, and $sl_PSSCH_DMRS_TimePatternList = 3$.

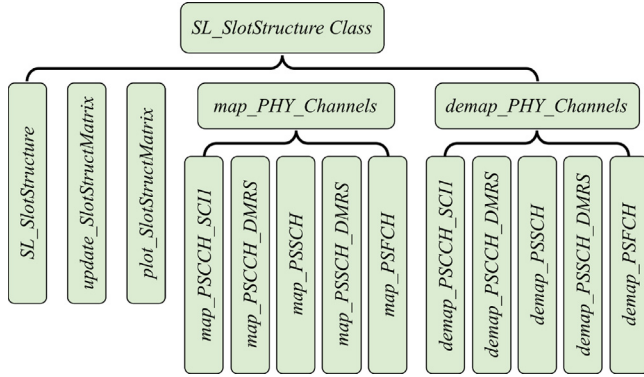


Fig. 7. Structure of the $SL_SlotStructure$ class.

structure is implemented in the $sl_generateTransmitSignal$ function after the modulations of the corresponding bit sequences. At the receiver, the OFDM demodulation is implemented in the $sl_processReceiveSignal$ function, and its output is written to the RX slot structure matrix. The demapping functions in the $SL_SlotStructure$ class are developed to demap either each physical channel or reference signal separately, or all of them can be demapped in one function. In the implementation, however, as we assume approximately perfect channel knowledge, only the demapping of SCI2 and data is implemented by modifying the original demapping functions of the Vienna simulator in order to comply with its channel estimation requirement.

3.3. Data and control multiplexing

Per 3GPP specifications, in 5G NR sidelink, data and SCI2 are multiplexed together after channel coding and rate matching on the raw bit sequences. The multiplexed bits are then scrambled with the scrambling sequence. The output sequence of the data and control multiplexing process is completed by concatenating the coded SCI2 bits with the coded data bits, and its format is determined by $nLayer$.

If the coded SCI2 and coded data bit sequences have the lengths of m and n , and

$$\begin{aligned} codedSCI2Bits: & b_0 b_1 \dots b_{m-1}, \\ codedDataBits: & d_0 d_1 \dots d_{n-1}, \end{aligned}$$

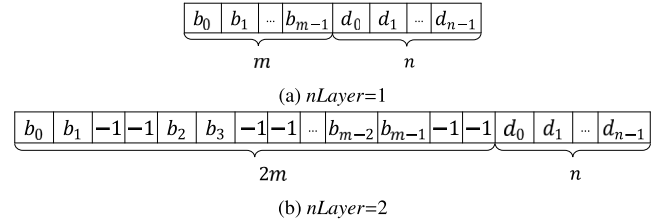


Fig. 8. Multiplexed bit sequence for different $nLayer$ values.

the multiplexed bit sequence ($multiplexedBits$) is shown in Fig. 8(a) when the number of data streams ($nLayer$) is 1, and in Fig. 8(b) when $nLayer$ is 2. Considering the SCI2 messages for both layers are identical in the two-layer scenario, and the modulation scheme for SCI2 is QPSK, every two groups of two coded SCI2 bits are interleaved by a group of $[-1, -1]$, which, during scrambling processing, are then replaced by the group of two scrambled bits before it.

At the receiver, the demultiplexing of data and control follows the descrambling procedure, and the demultiplexed SCI2 and data bits then go through rate recovery and channel decoding. It is worth noting that as two SCI2's are received in the 2-layer scenario, to improve the decoding performance, we keep both SCI2s for rate recovery and channel decoding.

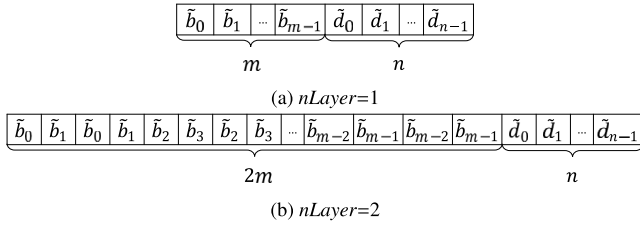
The data and control multiplexing and demultiplexing are implemented by the $sl_multiplex$ and $sl_demultiplex$, and they process the corresponding data in $sl_generateTransmitSignal$ and $sl_processReceiveSignal$, respectively.

3.4. PSSCH scrambling

The scrambling on PSSCH is performed between the multiplexed sequence and the scrambling sequence $c(n)$ before modulation. The format of the scrambled sequence differs with $nLayer$.

The multiplexed sequence before scrambling is shown in Figs. 8(a) and 8(b) for one-layer and two-layer scenarios, respectively. When scrambling is performed, each bit in b and d scrambles with the corresponding bit in $c(n)$:

$$\begin{aligned} \tilde{b}_n &= (b_n + c(n)) \bmod 2, \\ \tilde{d}_n &= (d_n + c(n)) \bmod 2. \end{aligned} \quad (8)$$

Fig. 9. Scrambling on PSSCH for different $nLayer$ values.

In a one-layer scenario, the scrambled sequences of \tilde{b} and \tilde{d} are concatenated in the same format as in Fig. 8(a). The scrambled format is shown in Fig. 9(a). In a two-layer scenario, however, each $[-1, -1]$ group shown in Fig. 8(b) is replaced by the group of two scrambled SCI2 bits before it. The scrambled format is shown in Fig. 9(b). The PSSCH scrambling is realized by the function $sl_scrambling$.

At the receiver, the PSSCH descrambling follows the demodulation of the received symbols. The descrambling reverses the procedures for scrambling and outputs the descrambled sequence with the same format as in Fig. 8(a) in the one-layer scenario. In the two-layer scenario, the descrambled SCI2 bits for Layer 2 are saved for decoding, instead of being replaced by $[-1, -1]$ groups. It is important to note that, as the demodulated sequence is in the form of Log-Likelihood Ratio (LLR), the descrambling is also performed by converting the corresponding scrambling sequence to the LLR form.

The scrambling sequence $c(n)$ is generated by two length-31 Gold sequences [17]:

$$c(n) = (x_1(n + 1600) + x_2(n + 1600)) \bmod 2, \quad (9)$$

where $x_1(n)$ is initialized by

$$x_1(n) = \begin{cases} 1 & n = 0, \\ 0 & n = 1, 2, \dots, 30, \end{cases} \quad (10)$$

and

$$\sum_{i=0}^{30} x_2(i) \cdot 2^i = c_{init}. \quad (11)$$

c_{init} is related to the 24-bit Cyclic Redundancy Check (CRC) on PSSCH p [17,18]:

$$\begin{aligned} c_{init} &= 2^{15} N_{ID} + 1010, \\ N_{ID} &= N_{ID}^X \bmod 2^{16}, \\ N_{ID}^X &= \sum_{i=0}^{L-1} p_i \cdot 2^{L-1-i}, L = 24. \end{aligned} \quad (12)$$

In the simulator, the generation of scrambling sequence is completed by the function $sl_scrambleSequence$. p and the length of the scrambling sequence are the inputs to the function. As the coded sequences of SCI2 and data share the scrambling sequence with the same c_{init} but different lengths, $c(n)$ is generated with the length of the longer of these two sequences. The first 31 bits in each of $x_1(n)$ and $x_2(n)$ are generated with bitwise operation in binary to avoid the computation complexity in decimal.

3.5. Sidelink layer mapping and precoding

Different from LTE sidelink where no spatial multiplexing is supported, NR sidelink supports MIMO transmission up to two layers. Accordingly, layer mapping and precoding will be implemented after modulation on the scrambled PSSCH bit sequence. The layer mapping procedure splits the modulated symbol sequence according to $nLayer$, and the precoding scales the symbols in each layer and maps each layer to its corresponding antenna port.

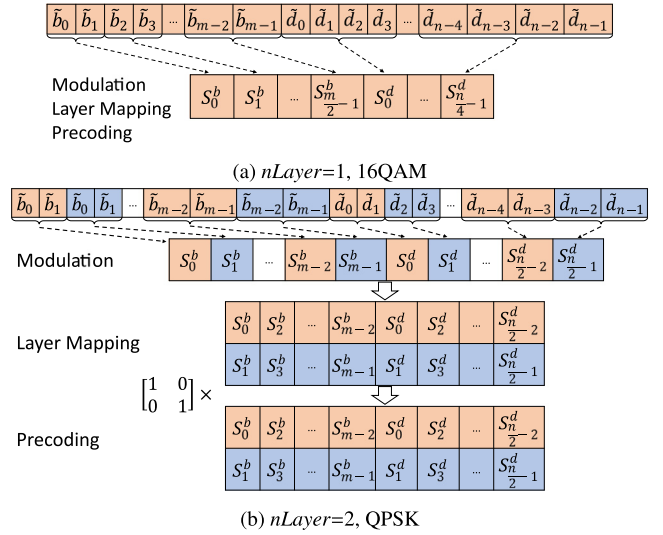


Fig. 10. Sidelink layer mapping and precoding for one-layer and two-layer scenarios.

In a one-layer scenario with modulation order Q for data bits, the first $m/2$ symbols of the modulated symbol sequence S are SCI2 symbols S^b , and the last n/Q symbols are data symbols S^d . S is mapped to a single layer, and the precoding has an identity precoding matrix of $W = 1$. Fig. 10(a) illustrates an example of the procedures from scrambled bit sequence to a one-layer precoded symbol sequence, with the data modulation of 16 Quadrature Amplitude Modulation (QAM) ($Q = 4$).

In a two-layer scenario, the first m symbols of S are SCI2 symbols S^b , where S_k^b with $k = 0, 2, \dots, m-2$ are mapped to Layer 1, and those with $k = 1, 3, \dots, m-1$ are mapped to Layer 2. The last n/Q symbols are data symbols S^d , where S_k^d with $k = 0, 2, \dots, n/Q-2$ are mapped to Layer 1, and those with $k = 1, 3, \dots, n/Q-1$ are mapped to Layer 2. The layer mapped sequence is then multiplied with the identity precoding matrix W :

$$\begin{aligned} Z &= WS, \\ W &= \begin{bmatrix} 1 & 0 \\ 0 & 1 \end{bmatrix}. \end{aligned} \quad (13)$$

The two-layer procedures from scrambled bit sequence to precoded symbol sequence are shown in Fig. 10(b), with the data modulation of QPSK ($Q = 2$).

In the LLS, layer mapping and precoding are implemented in the $sl_generateTransmitSignal$ function, and the precoding matrix is defined in the $SidelinkScenario$ script.

3.6. Error-free and error-prone SCI2

In physical layer design and performance evaluation, the performance of control signaling transmission, such as PSSCH and SCI2, is often an interesting topic for researchers. In addition, in link-to-system mapping, there are often various requests on BLER-to-SNR mapping, such as control only, data only, or integrated control and data. For this purpose and to provide flexible options, our sidelink simulator provides the options of (1) error-free SCI2, which separates the data collection and processing of SCI2 from decoding of a Transport Block (TB), and (2) error-prone SCI2, where a TB cannot be decoded properly if the associated SCI2 is not received correctly.

In the error-free SCI2 scenario, the decoding of a data transmission is under the assumption that the SCI2 is decoded without error. The data transmission in each slot is decoded, and the BLER is recorded by summarizing the decoding results of each TB transmission(s). The BLER of SCI2 transmission is also recorded separately, and its BLER is

calculated by summarizing the decoding result of SCI2 in each slot. The error-free SCI2 scenario can be enabled in the *SidelinkScenario* script.

When the error-prone SCI2 scenario is enabled, if the decoding of SCI2 in a slot returns an error, the decoding of this TB transmission is skipped and automatically recorded as erroneous. The decoding error of SCI2 transmissions in this scenario is still recorded for each slot, whereas the decoding error of TB transmission(s) reflects the error from both SCI2 and TB transmissions.

3.7. Blind-based and feedback-based HARQ

To increase reliability of TB transmissions, for unicast, 5G NR sidelink supports both blind-based HARQ and feedback-based HARQ, and the maximum number of transmissions is configurable and up to 32 [20]. In blind-based HARQ, a transmitter UE transmits one TB for a certain number of times without requiring any HARQ feedback. Whereas in feedback-based HARQ, a transmitter UE retransmits the TB after receiving a NACK or no response after a predefined time, up to the configured maximum number of transmissions. Apparently, on one hand, feedback-based HARQ can prevent unnecessary retransmissions that would otherwise waste sidelink resources and increase the channel load. On the other hand, feedback-based HARQ requires feedback that occupies sidelink resources and could potentially increase latency. In our LLS, blind-based or feedback-based HARQ is set as one scenario parameter, which is used later in the resource pool object.

Per 3GPP [19], HARQ feedback for a TB sent on a PSSCH in a resource pool is carried on a PSFCH within the same resource pool. Resources for PSFCH can be (pre-)configured periodically with a period of $N = 1, 2$, or 4 slot(s), i.e., there is a slot with PSFCH every N slots [20]. To disable the HARQ feedback for a specific TB, the value of 0 can be set to the HARQ feedback enabled/disabled indicator field in the corresponding SCI2 [18]. To disable the HARQ feedback for all sidelink transmissions in the resource pool, no resources for PSFCH are configured [20]. In the LLS, PSFCH configuration is realized in the resource pool object. Since the focus of the LLS is one point-to-point link, HARQ feedback is not enabled/disabled at the TB level, but rather at the resource pool level.

In addition, to accommodate the processing delay at the receiver UE, in 3GPP [20], a time gap $sl_MinTimeGapPSFCH$ between the PSSCH and the PSFCH is configured in the time domain, with a single value of 2 or 3 per resource pool. The receiver UE transmits the PSFCH in the first slot that includes PSFCH resources and is at least $sl_MinTimeGapPSFCH$ slots in the resource pool after the last slot of the PSSCH reception. In the LLS, this time gap is implemented in the resource pool object, and is also used in the resource allocation mechanism to ensure the minimum time gap between the associated PSSCH and PSFCH.

Given that the focus of the LLS is one point-to-point link instead of scheduling algorithms, the LLS implements a simple resource allocation mechanism. For blind-based HARQ, all transmissions of one TB are transmitted in consecutive slots. For feedback-based HARQ, note that the number of symbols available to PSSCH differs between a slot with PSFCH and a slot without PSFCH (Figs. 5 and 6). This means that the sizes of the TBs that these two types of slots can hold are different. In the LLS, if the initial transmission of one TB is on a slot with PSFCH, all its retransmissions are scheduled in slots with PSFCH, and vice versa.

To avoid waste of resources while waiting for HARQ feedback, 3GPP further allows multiple simultaneous outstanding TBs [23], and HARQ process IDs are used to identify these TBs. The number of HARQ process IDs can be a maximum of 16 in sidelink Mode 1 and a maximum of 4 in sidelink Mode 2. Moreover, different copies of the same TB are combined at the receiving UE based on their redundancy versions, and each redundancy version is generated by shifting the starting position of the bit sequence after LDPC encoding [18]. In the LLS, a sidelink HARQ entity is developed to manage HARQ processes and redundancy versions, as illustrated in Fig. 11. As shown in the figure,

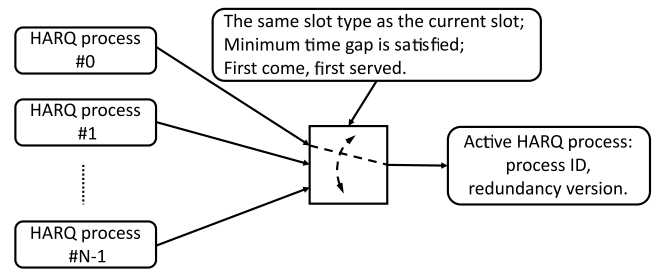


Fig. 11. HARQ Management.

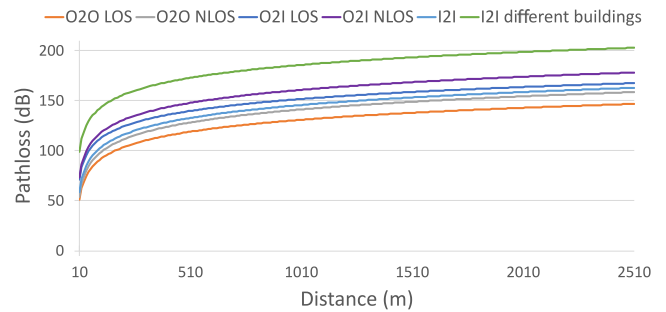


Fig. 12. LTE D2D pathloss models for different deployment environment.

the active HARQ process is selected based on whether its associated slot type (with or without PSFCH) matches the current slot and whether the minimum time gap between its associated PSSCH and PSFCH is satisfied. If both conditions are satisfied, the process that has been waiting for a longer time in the buffer will be chosen. After the active HARQ process is selected, the next redundancy version of the associated TB is transmitted.

3.8. Communication range and performance evaluation

Communication range is one major topic in wireless communications and of special interest since the beginning of D2D communications. In this context, communication range refers to the maximum distance between a transmitter and a receiver such that the transport block transmitted could be received with an error probability not exceeding the Target Loss Rate (TLR). In addition, other performance metrics at the border of the communication range, such as target SNR, throughput, and latency, can also be evaluated. This section introduces how the SL LLS evaluates these performance metrics.

By using the pathloss models defined by 3GPP, the communication range evaluation feature allows our SL LLS to give range numbers directly from link-level simulations. Channel models for D2D are defined in 3GPP specifications for ProSe under LTE [24], which include three deployment scenarios: Outdoor-to-Outdoor (O2O), Outdoor-to-Indoor (O2I), and Indoor-to-Indoor (I2I). In each of the O2O and O2I scenarios, both Line-of-Sight (LOS) and Non-Line-of-Sight (NLOS) cases are specified. In the I2I scenario, only NLOS case is considered, and an additional penetration loss can be added when more than one obstacle is involved. This gives six deployment scenarios in total. Fig. 12 provides the distance-vs-pathloss curves at band n14 for all these six scenarios, where the curve marked with “I2I different buildings” maps to the scenario of I2I with additional penetration loss added.

Fig. 13 shows the functions that convert simulation parameters into communication range and other performance metrics at the border of the communication range, which include target SNR, throughput, and latency. They are evaluated by the *getRangeParameters* function, using the designated target loss rates and simulation results. The *getRangeParameters* function calls the *getDistanceFromPathloss* function, which is

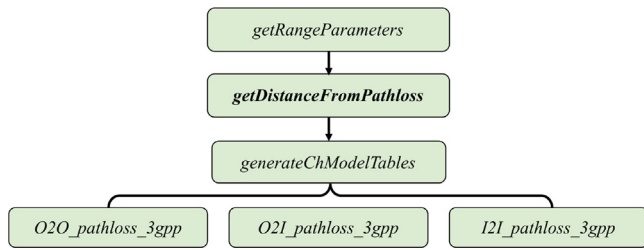


Fig. 13. Functions for the communication range and performance evaluation.

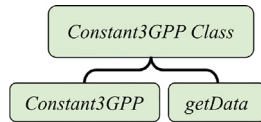


Fig. 14. Structure of the *Constant3GPP* class for constant management [25].

the major function in this feature, to calculate the communication range at each designated target loss rate. It returns the corresponding distance according to the specified values of pathloss, which is calculated using the total pathloss in simulation and the noise figure, and deployment environment. When the function is executed for the first time, *getDistanceFromPathloss* calls *generateChModelTables* to generate the lookup tables for the six scenarios. These lookup tables are generated by *O2O_pathloss_3gpp*, *O2I_pathloss_3gpp*, and *I2I_pathloss_3gpp*. When a lookup table is used in *getDistanceFromPathloss* and the pathloss value happens to be absent, interpolation is used to estimate the corresponding distance,

3.9. Constant management

3GPP standards specify a significant number of constant values. Such constants are often presented using tables, and may be subject to update following 3GPP meetings. To help researchers keep track of updates on constants and their values without roaming through the code to make modifications, the *Constant3GPP* class is developed, as shown in Fig. 14 [25].

Each of the tables used in the simulator is created in a table under a unique function. Users can update the tables when new updates are available in the 3GPP standards. The name of the function is added to the cell array of *dataList* under the *Constant3GPP* class. By running the *getData* function, *dataList* accesses the table of interest in the form of an anonymous function [25]. In addition, when other tables in the 3GPP standards are needed, users can create another unique function following the existing examples. After adding the new function name to *dataList*, the data will also be available to the *getData* function.

3.10. Adaptive sweeping value selection

To generate the desired outputs, researchers often face the challenge of setting an appropriate range of values for an input simulation parameter. This process can be time-consuming as determining the suitable value range typically requires manual trial and error, particularly when simulating a single data point takes a significant amount of time, which could even make it unrealistic to run batch executions [25].

The adaptive sweep function focuses on addressing this challenge and automating the execution process by:

1. setting a range for the input parameter that is large enough to encompass values to generate the desired outputs, as well as the granularities for both the input and output based on acceptable accuracies. This is realized by the constructor function *adaptiveSweep* of the *adaptiveSweep* class, as illustrated in Fig. 15.

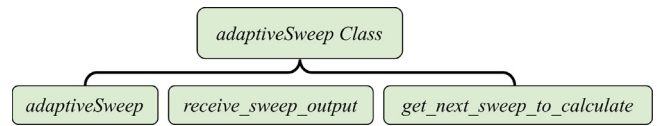


Fig. 15. Structure of the *adaptiveSweep* class [25].

2. receiving the output values for the end points of the input range, and adaptively preparing the parameters needed for searching for the next input range. This is realized by the *receive_sweep_output* function. And
3. using a “divide and conquer” strategy to determine the next input value. This is realized by the *get_next_sweep_to_calculate* function.
4. continuing the above steps until the configured granularities for the input and output are reached, which ensures the desired accuracies [25].

In addition, the adaptive sweep function also allows for designating a Point of Interest (POI) and its granularity, where a series of input values around the POI can be generated with a finer granularity, which leads to a higher accuracy around the POI [25].

This feature is currently designed to focus on the parameters in our communication range research topic. However, it can be easily modified and customized to fit other research purposes, which can significantly save a researcher’s time and effort in implementing simulations [25].

4. Simulation results

In this section, we illustrate the versatility of the SL LLS in addressing various research topics. We also present several results derived from the simulations. The simulations are performed on one point-to-point link at public safety band n14, which uses center frequency 795 MHz and Frequency Division Duplex (FDD), with one power class 3 transmitter UE (transmit power 23 dBm) and one receiver UE. Unless mentioned otherwise, other simulation parameters are set as follows. Numerology is set to 0, O2O LOS pathloss model is used with Additive White Gaussian Noise (AWGN) channel, and noise figure is set to 9 dB. 10 PRBs are allocated for data transmissions and MCS corresponding to Channel Quality Indication (CQI) 1 is deployed. It is worth noting that as the modulation order, target coding rate, and spectral efficiency for each CQI index are mapped to their counterparts for a MCS index in the corresponding tables, we use CQI index to represent MCS in the SL LLS. For HARQ, unless mentioned otherwise, blind-based HARQ is configured by default, and the maximum number of transmissions is set to 1. Accordingly, PSFCH is disabled. Also, error-free SCI2 and perfect channel knowledge are assumed.

4.1. Error-free SCI2 vs error-prone SCI2

As introduced in Section 3.6, to support the study of control signaling transmission and to facilitate link-to-system mapping, our SL LLS supports both error-free SCI2 and error-prone SCI2. In this simulation, we use our SL LLS to investigate the impact of error-prone SCI2 on TB decoding. We implemented this simulation set by toggling the error-prone SCI2 option for all the CQI indexes of Table 5.2.2.1-2 in [23], and each simulation runs for 10000 slots. The resulting BLER curves are shown in Fig. 16.

In Fig. 16, each pair of curves with the same color represents the TB BLERs of one CQI, with solid lines and dotted lines representing the error-free SCI2 scenario and the error-prone SCI2 scenario, respectively. It can be observed that, for each pair, the solid line is slightly on the left side of the dotted line, indicating a better performance in the error-free SCI2 scenario. Nevertheless, the difference is barely visible. It indicates

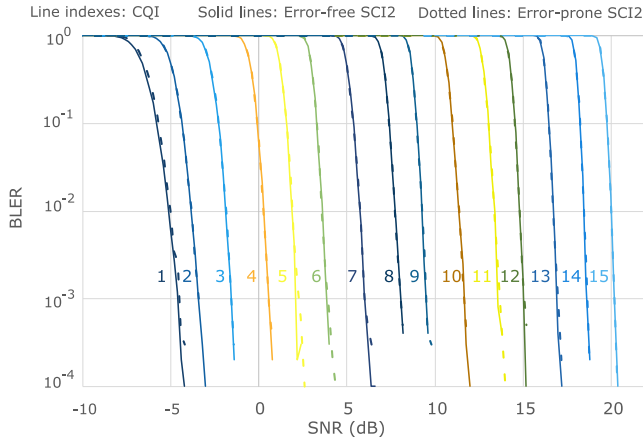
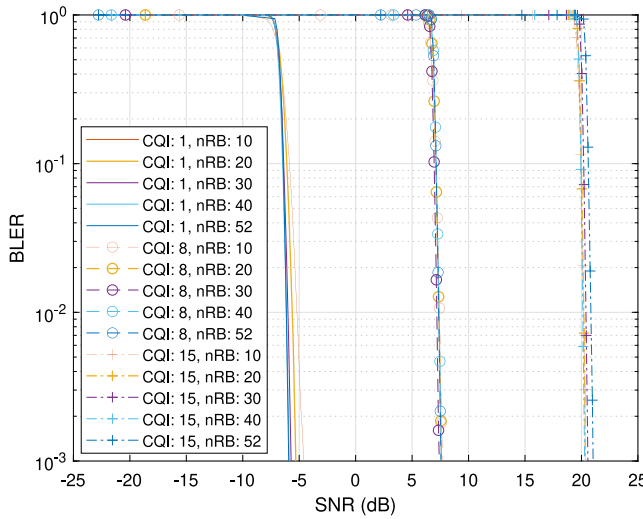


Fig. 16. BLER curves for error-free SCI2 and error-prone SCI2.

Fig. 17. BLER curves for different numbers of RBs allocated with CQI = 1, 8, and 15, at $\mu = 0$.

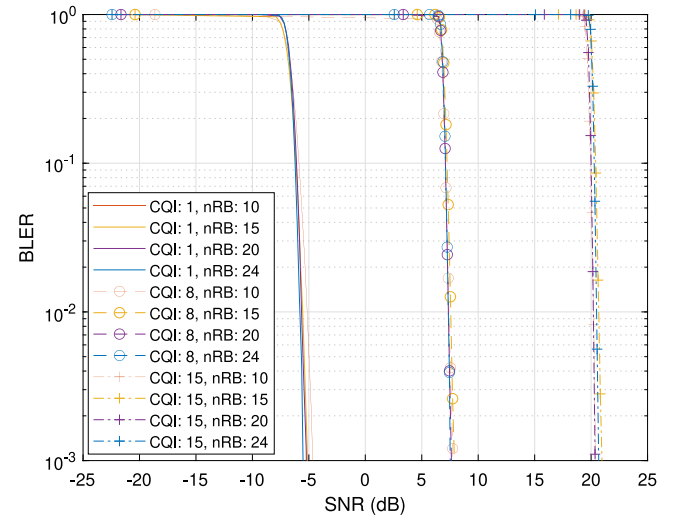
that under the same channel condition, the impact of error-prone SCI2 decoding on the decoding of a TB is insignificant. This is consistent with the design of control signaling, which uses polar coding and QPSK and is required to be more robust due to its importance.

4.2. Impact of number of allocated RBs

At Band n14, the number of allocated RBs could range from 10 to 52 at $\mu = 0$ and from 10 to 24 at $\mu = 1$. It is beneficial to understand the impacts of the number of allocated RBs on the BLER curves, especially for the purpose of narrowing down BLER curve sets for PHY abstraction and link-to-system mappings. In this section, we demonstrate the BLER curve shifts with changes in the number of allocated RBs. Simulation for each point runs for 10000 slots. Furthermore, we repeated the simulation by changing CQI from 1 to 8 and 15 to investigate potential impacts of CQI on BLER shifts.

Fig. 17 indicates that at $\mu = 0$ and CQI = 1, the BLER performance improves when increasing number of allocated RBs. The maximum difference in SNR is relatively small and is around 1 dB at TLR = 0.5%. This trend at CQI = 1 is also observed when $\mu = 1$, as shown in Fig. 18, where the maximum SNR difference is around 0.7 dB at TLR = 0.5%.

Similar to the case of CQI = 1, Fig. 17 shows that the BLER curves for CQI = 8 or 15 do not shift significantly with the number of RBs allocated at $\mu = 0$. The maximum SNR differences are less than 0.5 dB

Fig. 18. BLER curves for different numbers of RBs allocated with CQI = 1, 8, and 15, at $\mu = 1$.

at TLR = 0.5%, and the BLER curves do not shift towards lower SNR with increasing number of RBs allocated. This observation also applies to CQI = 8 and 15 at $\mu = 1$.

Figs. 17 and 18 also demonstrate that with CQI increasing, a higher SNR is required to achieve the same BLER. This result is also observed in Fig. 16 and meets our expectation.

The data above shows that although at a low CQI, the BLER curves shift towards lower SNRs when the number of allocated RBs increases, the maximum shift is no higher than 1 dB. The impact of number of allocated RBs is hence insignificant, and the BLER curves under different number of allocated RBs could be potentially combined into one in PHY abstraction and link-to-system mappings, which could reduce the complexity significantly without loss of accuracy. This conclusion is further supported by the simulation results from higher CQIs, where the differences in BLER curve shifts are barely noticeable.

4.3. Deployment environment on communication range

Public safety communications is one major application of sidelink and D2D communications, and the deployment environment involved can be complicated especially for rescues after disasters. It is of great value for first responders to have the knowledge of communication ranges in a certain deployment environment.

For this purpose, we conducted link-level simulations in three scenarios: O2O, O2I, and I2I. For O2O, depending on whether obstruction is along the path, both LOS and NLOS propagations are simulated. For O2O LOS, we select AWGN channel for comparison. As communication in both O2O LOS and O2O NLOS environments may be initiated from a pedestrian or a vehicular, we select the PDPs of Pedestrian B and Vehicular B as small scale channel models. The simulations are conducted by changing these corresponding parameters in the functions discussed in Section 3.8. The results are shown in Fig. 19.

As shown in Fig. 19, the deployment achieves the longest communication range with AWGN channel. As AWGN is the simplest channel model, this result is expected. For both LOS and NLOS propagation, the deployments for pedestrian show better performance than those for vehicular. This is due to the higher Doppler shift coming from the vehicle's speed. With the same channel model, LOS propagation provides a longer communication range than NLOS propagation, as signal propagation experiences higher path loss with NLOS.

In the O2I scenario, NLOS propagation is simulated for both Vehicular B and Pedestrian B channel models, as obstruction exists in most

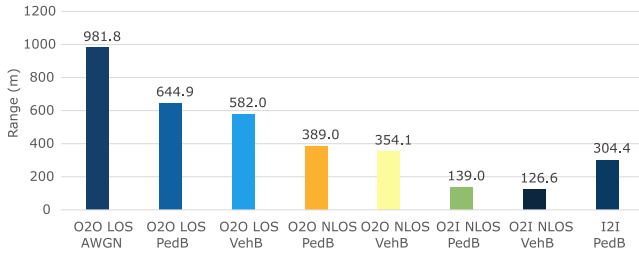


Fig. 19. Communication range evaluation under different deployment environment.

cases. The simulation results demonstrate a better performance with Pedestrian B, which aligns with the O2O scenario.

In the I2I scenario, only Pedestrian B channel model is applied, as communication that involves a vehicular is a less likely scenario. Compared to O2I, the simulation result for I2I (within the same building) shows a significantly longer communication range. As O2I has much higher penetration loss, the performance is also expected.

The data shows that for the baseline configuration, although the ideal communication range can reach 981.8 m under an ideal deployment environment, the actual communication range can vary depending on the deployment environment where the communication experiences. When more penetration loss and higher Doppler shift occur, the performance may drop to 126.6 m or even lower. Therefore, the deployment environment for NR sidelink needs to be carefully taken into account when predicting the potential connectivity.

4.4. Performance under different numerology and UE power class

5G NR introduces flexible numerology (μ) to support a variety of services with different performance requirements. This changes the resource grid in both time and frequency domains. For example, in frequency domain, the SCS is 15 kHz for $\mu = 0$ and 30 kHz for $\mu = 1$. As we set $sl_RB_Number = 10$, the bandwidth when $\mu = 1$ is twice than that when $\mu = 0$. Meanwhile, in time domain, the time duration of a slot is 1 ms for $\mu = 0$ and 0.5 ms for $\mu = 1$. In this simulation, we explore the impacts of numerology on the required SNR, communication range, throughput, and latency for both $\mu = 0$ and 1, at a TLR of 0.5%. Note that the throughput and latency reported are measured at the border of the communication range. Also note that as mentioned in Section 2, latency here is a simplified version that refers to the difference from the time a data packet is transmitted at the transmitter to the time it is received successfully at the receiver, and does not include other delays such as processing delay.

Fig. 20 shows that at a TLR of 0.5%, the required SNRs for $\mu = 0$ and 1 are the same. The SNRs can be converted to pathloss values by combining transmitting power, noise figure, bandwidth, and operating temperature. As $\mu = 1$ has a larger SCS and bandwidth, its signal power is more dispersed.

From the function introduced in Section 3.8, a shorter communication range is expected. This is consistent with Fig. 20.

In terms of throughput, both cases share the same $nPRB$ but SCS is doubled in case of $\mu = 1$. The resource utilized in case of $\mu = 1$ is hence doubled, and the throughput is therefore expected to be around twice as that for $\mu = 0$. This derivation is reflected in Fig. 20. Likewise, as a TB is decoded in the same slot as it is transmitted, using our simplified version of latency without considering other delays, the latency for $\mu = 1$ is expected to be around half of that for $\mu = 0$, which is also reflected in Fig. 20.

The above simulation data shows how numerologies influence the performance metrics towards different directions. That is, careful sidelink configurations are required to meet a variety of service needs, which aligns with the goal of introducing numerology in 5G.

The power class for a UE is default at Power Class 3, which is 23 dBm. In addition, 3GPP standard [21] specifies high power class

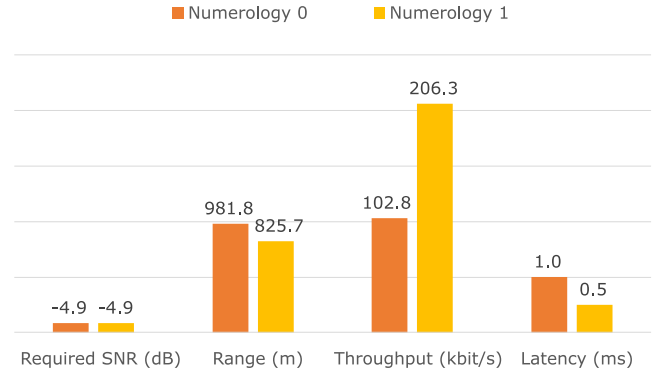


Fig. 20. Impacts of numerology on required SNR, communication range, throughput, and latency (numerology 0 and 1, at TLR = 0.5%).

Table 2

Communication ranges at different UE power classes for numerologies 0 and 1.

Power class	Communication range	
	$\mu = 0$	$\mu = 1$
Power Class 3 (23 dBm)	981.8 m	825.7 m
Power Class 1 (31 dBm)	1554.4 m	1311.9 m

for Band n14, which is Power Class 1 with 31 dBm signal power. The additional power a UE can provide will improve the communication ranges at both $\mu = 0$ and 1.

Table 2 summarizes the communication range evaluations for the allowed UE power classes at numerologies 0 and 1. Both scenarios show significant improvements in communication range when power increases, where the improvement is around 573 m at $\mu = 0$, which is 58 % increase. Such improvement is around 486 m or 59 % at $\mu = 1$.

In addition, we can also observe from Table 2 that at Power Class 1, the communication range is also shorter at a higher numerology. This aligns with the observation in the previous numerology analysis shown in Fig. 20.

4.5. Performance under enhanced NR sidelink HARQ mechanism

Since the start of sidelink and D2D communications, communication range has been one major topic of interest. While LTE sidelink supports blind-based HARQ with four mandatory transmissions, 5G NR sidelink supports both blind-based and feedback-based HARQ, and allows up to 32 transmissions. This brings a great potential to improve sidelink communication range. On the other hand, the latency of a packet transmission increases as the number of HARQ transmissions increases. In this simulation, we use our sidelink simulator to study the communication range and the corresponding latency under different HARQ configurations. Note that, similar to previous data, the latency here is the simplified version and maps to experience at the border of communication range. Also, the intention of this study is to explore the link-level performance. Hence, the latency considered here is not bounded by other high layer operations such as scheduling algorithms.

For this purpose, for both blind-based and feedback-based HARQ, we set the maximum number of transmissions to be 1, 4, 8, 16, and 32, respectively. In the feedback-based HARQ simulation, we enable PSFCH transmissions with a PSFCH period of 4. The corresponding range and latency can be calculated from the BLER curves at a TLR of 0.5%. The results for both blind-based and feedback-based HARQ are plotted in Fig. 21.

The range curves in Fig. 21 show a significant improvement in range values with increasing number of transmissions, for both blind-based and feedback-based HARQ. This is consistent with our expectation, as a higher number of (re)transmissions increases the TB decoding success

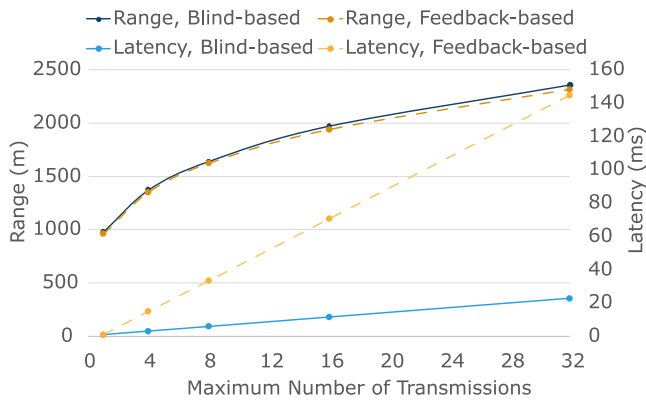


Fig. 21. Communication range and latency for blind-based HARQ and feedback-based HARQ, at TLR = 0.5%.

rate. The link can hence tolerate a higher path loss, which leads to a longer range.

However, the latency curves in Fig. 21 clearly show a significant increase in latency. The latency can be as high as around 140 ms, which would fail many applications. Also, as retransmission in feedback-based HARQ only happens after a corresponding PSFCH is received, its latency is expected to be significantly higher than the latency for blind-based HARQ, especially when the maximum number of transmissions is high. Fig. 21 shows that the latency for feedback-based HARQ can be up to 122 ms longer than that of blind-based HARQ.

This data shows that NR sidelink enhanced HARQ can indeed improve communication range significantly. However, a careful design is required to balance other performance metrics, such as latency, in order to meet various service needs.

5. Conclusion

In this paper, we have presented a 5G NR sidelink link-level simulator that we have developed and made publicly accessible [15]. The simulator conforms closely to 3GPP specifications on NR sidelink and supports various NR sidelink features such as sidelink BWP and resource pool, sidelink slot format including feedback channel and two-stage SCIs, data and control multiplexing, data and SCI2 scrambling, sidelink layer mapping and precoding, blind- and feedback-based HARQ, and communication range evaluation. It is modular and adaptable to different link-level simulations of interest.

Using our simulator, we have investigated the impact of different sidelink parameters on sidelink performance. Our simulation results indicate that the BLER curve shifts are insignificant when comparing error-prone SCI2 and error-free SCI2, and the impact of the number of allocated RBs is also insignificant. Additionally, different deployment environments can result in significant gaps in communication range. Moreover, while configuring numerology 0 and 1 offers a trade-off between communication range, throughput, and latency, high power class UE significantly increases communication range. Furthermore, while 5G NR sidelink enhanced HARQ mechanism can indeed improve communication range significantly, a careful design is required to balance other performance metrics, such as latency, in order to meet various service needs. Our simulator is the first publicly accessible 5G NR sidelink link-level simulator and can be used to further investigate the performance of 5G NR sidelink under various scenarios.

The current version of the simulator is designed for a single point-to-point sidelink with FDD and data transmissions and with partial implementation of control and feedback channels. The simulator focuses on performance metrics BLER curves, communication range, throughput and latency. In our future releases we plan to extend it to include full implementation of control channel and feedback channel,

as well as other performance metrics such as BER and FER. We also plan to expand the simulator to include Time Division Duplex (TDD) transmission and link-level simulation at V2X frequency bands. Additionally, we aim to develop PHY abstraction to integrate the link-level data into system-level simulations.

Declaration of competing interest

The authors declare that they have no known competing financial interests or personal relationships that could have appeared to influence the work reported in this paper.

Data availability

The code for the sidelink link-level simulator is available online. Please find the link in the References

Acknowledgments

The authors thank Tom Henderson (University of Washington) for insightful technical discussions and guidance throughout the project, and Jean-Aicard Fabien (National Institute of Standards and Technology) for providing timely support on 3GPP specifications and their developments.

References

- [1] S.-Y. Lien, D.-J. Deng, C.-C. Lin, H.-L. Tsai, T. Chen, C. Guo, S.-M. Cheng, 3GPP NR sidelink transmissions toward 5G V2X, *IEEE Access* 8 (2020) 35368–35382, <https://doi.org/10.1109/ACCESS.2020.2973706>.
- [2] M.H.C. Garcia, A. Molina-Galan, M. Boban, J. Gosalvez, B. Coll-Perales, T. Şahin, A. Kousaridas, A tutorial on 5G NR V2X communications, *IEEE Commun. Surv. Tutor.* 23 (3) (2021) 1972–2026, <https://doi.org/10.1109/COMST.2021.3057017>.
- [3] F. Cintron, D. Griffith, C. Liu, R. Rouil, Y. Sun, J. Wang, P. Liu, C. Shen, A.B. Mosbah, S.G. Quintiliani, Study of 5G New Radio (NR) Support for Direct Mode Communications, NIST Interagency/Internal Report (NISTIR), National Institute of Standards and Technology, Gaithersburg, MD, 2021, <https://doi.org/10.6028/NIST.IR.8372>.
- [4] M. Harounabadi, D.M. Soleymani, S. Bhadauria, M. Leyh, E. Roth-Mandutz, V2X in 3GPP standardization: NR sidelink in release-16 and beyond, *IEEE Commun. Stand. Mag.* 5 (1) (2021) 12–21, <https://doi.org/10.1109/MCOMSTD.001.2000070>.
- [5] The MathWorks Inc., LTE toolbox user's guide, 2022, https://www.mathworks.com/help/pdf_doc/lte/lte Ug.pdf. (Accessed: 18 June 2022).
- [6] The MathWorks Inc., 5G toolbox user's guide, 2022, https://www.mathworks.com/help/pdf_doc/5g/5g Ug.pdf. (Accessed: 18 June 2022).
- [7] S. Pratschner, B. Tahir, L. Marijanovic, M. Mussbah, K. Kirev, R. Nissel, S. Schwarz, M. Rupp, Versatile mobile communications simulation: The vienna 5G link level simulator, *EURASIP J. Wireless Commun. Networking* 2018 (1) (2018) 226, <https://doi.org/10.1186/s13638-018-1239-6>.
- [8] Z. Ali, S. Lagén, L. Giupponi, R. Rouil, 3GPP NR V2X mode 2: Overview, models and system-level evaluation, *IEEE Access* 9 (2021) 89554–89579, <https://doi.org/10.1109/ACCESS.2021.3090855>.
- [9] University of Surrey, Link level simulator, 2022, <https://www.surrey.ac.uk/institute-communication-systems/facilities/link-and-system-level-simulators>. (Accessed: 18 June 2022).
- [10] S. Cho, S. Chae, M. Rim, C.G. Kang, System level simulation for 5G cellular communication systems, in: 2017 Ninth International Conference on Ubiquitous and Future Networks, ICUFN, 2017, pp. 296–299, <https://doi.org/10.1109/ICUFN.2017.7993797>.
- [11] T.R. Henderson, M. Lacage, G.F. Riley, Network simulations with the ns-3 simulator, in: *Sigcomm Demo*, 2008.
- [12] G. Piro, N. Baldo, M. Miozzo, An LTE module for the ns-3 network simulator, in: *Proceedings of the 4th International ICST Conference on Simulation Tools and Techniques, SIMUTools '11*, ICST (Institute for Computer Sciences, Social-Informatics and Telecommunications Engineering), Brussels, BEL, 2011, pp. 415–422.
- [13] N. Patriciello, S. Lagen, B. Bojovic, L. Giupponi, An E2E simulator for 5G NR networks, 2019, <https://doi.org/10.48550/ARXIV.1911.05534>, arXiv, URL <https://arxiv.org/abs/1911.05534>.
- [14] W. Donglin, R.R. Sattiraju, Q. Anjie, S. Partani, H.D. Schotten, Methodologies of link-level simulator and system-level simulator for C-V2X communication, 2019, <https://doi.org/10.48550/ARXIV.1907.04693>, arXiv.

- [15] National Institute of Standards and Technology, University of Washington, New radio sidelink simulator, 2022, <https://www.nist.gov/services-resources/software/new-radio-sidelink-simulator>. (Accessed: 02 September 2022).
- [16] P. Liu, C. Shen, C. Liu, F.J. Cintrón, L. Zhang, L. Cao, R. Rouil, S. Roy, 5G New Radio Sidelink Link-Level Simulator and Performance Analysis, in: MSWiM '22, Association for Computing Machinery, New York, NY, USA, 2022, pp. 75–84, <http://dx.doi.org/10.1145/3551659.3559049>.
- [17] 3GPP, NR; Physical Channels and Modulation (Release 16), (Technical Specification (TS) 38.211) 3rd Generation Partnership Project (3GPP), 2021, Version 16.6.0.
- [18] 3GPP TS38.212, 3rd Generation Partnership Project; Technical Specification Group Radio Access Network; NR; Multiplexing and channel coding, Standard 16.6.0, 3GPP, 2021.
- [19] 3GPP TS38.213, 3rd Generation Partnership Project; Technical Specification Group Radio Access Network; NR; Physical layer procedures for control, 16.6.0, 3GPP, 2021.
- [20] 3GPP TS38.331, 3rd Generation Partnership Project; Technical Specification Group Radio Access Network; NR; Radio Resource Control (RRC) Protocol Specification, 16.5.0, 3GPP, 2021.
- [21] 3GPP TS38.101-1, 3rd Generation Partnership Project; Technical Specification Group Radio Access Network; NR; User Equipment (UE) Radio Transmission and Reception; Part 1: Range 1 Standalone, 16.8.0, 3GPP, 2021.
- [22] 3GPP TS38.101-2, 3rd Generation Partnership Project; Technical Specification Group Radio Access Network; NR; User Equipment (UE) Radio Transmission and Reception; Part 2: Range 2 Standalone, 16.8.0, 3GPP, 2021.
- [23] 3GPP, NR; Physical Layer Procedures for Data (Release 16), 38.214, 3rd Generation Partnership Project (3GPP), 2020, Version 16.3.0.
- [24] 3GPP, Study on LTE Device to Device Proximity Services; Radio Aspects (Release 12), 36.843, 3rd Generation Partnership Project (3GPP), 2014, Version 12.0.1.
- [25] C. Liu, F.J. Cintron, R. Rouil, P. Liu, C. Shen, L. Zhang, L. Cao, S. Roy, 5G New Radio Sidelink Link-Level Simulator v1.0 User Manual, National Institute of Standards and Technology, 2022.